Geometric feature-based multimodal image registration of contrast-enhanced cardiac CT with gated myocardial perfusion SPECT

Jonghye Woo, Piotr J. Slomka,[a] Damini Dey, Victor Y. Cheng, Byung-Woo Hong, Amit Ramesh, Daniel S. Berman, Ronald P. Karlsberg, C.-C. Jay Kuo, and Guido Germano
Department of Imaging/AIM program, Cedars-Sinai Medical Center, Los Angeles, California 90048

(Received 22 May 2009; revised 21 September 2009; accepted for publication 29 September 2009; published 5 November 2009)

Purpose: Cardiac computed tomography (CT) and single photon emission computed tomography (SPECT) provide clinically complementary information in the diagnosis of coronary artery disease (CAD). Fused anatomical and physiological data acquired sequentially on separate scanners can be coregistered to accurately diagnose CAD in specific coronary vessels.
Methods: A fully automated registration method is presented utilizing geometric features from a reliable segmentation of gated myocardial perfusion SPECT (MPS) volumes, where regions of myocardium and blood pools are extracted and used as an anatomical mask to de-emphasize the inhomogeneities of intensity distribution caused by perfusion defects and physiological variations. A multiresolution approach is employed to represent coarse-to-fine details of both volumes. The extracted voxels from each level are aligned using a similarity measure with a piecewise constant image model and minimized using a gradient descent method. The authors then perform limited nonlinear registration of gated MPS to adjust for phase differences by automatic cardiac phase matching between CT and MPS. For phase matching, they incorporate nonlinear registration using thin-plate-spline-based warping. Rigid registration has been compared with manual alignment ($n=45$) on 20 stress/rest MPS and coronary CTA data sets acquired from two different sites and five stress CT perfusion data sets. Phase matching was also compared to expert visual assessment.
Results: As compared with manual alignment obtained from two expert observers, the mean and standard deviation of absolute registration errors of the proposed method for MPS were 4.3 ± 3.5, 3.6 ± 2.6, and 3.6 ± 2.1 mm for translation and $2.1\pm3.2°$, $0.3\pm0.8°$, and $0.7\pm1.2°$ for rotation at site A and 3.8 ± 2.7, 4.0 ± 2.9, and 2.2 ± 1.8 mm for translation and $1.1\pm2.0°$, $1.6\pm3.1°$, and $1.9\pm3.8°$ for rotation at site B. The results for CT perfusion were 3.0 ± 2.9, 3.5 ± 2.4, and 2.8 ± 1.0 mm for translation and $3.0\pm2.4°$, $0.6\pm0.9°$, and $1.2\pm1.3°$ for rotation. The registration error shows that the proposed method achieves registration accuracy of less than 1 voxel ($6.4\times6.4\times6.4$ mm) misalignment. The proposed method was robust for different initializations in the range from -80 to 70, -80 to 70, and -50 to 50 mm in the x-, y-, and z-axes, respectively. Validation results of finding best matching phase showed that best matching phases were not different by more than two phases, as visually determined.
Conclusions: The authors have developed a fast and fully automated method for registration of contrast cardiac CT with gated MPS which includes nonlinear cardiac phase matching and is capable of registering these modalities with accuracy <10 mm in 87% of the cases. © *2009 American Association of Physicists in Medicine*. [DOI: 10.1118/1.3253301]

Key words: multimodal image registration, myocardial perfusion SPECT, coronary CTA

I. INTRODUCTION

The common use of multiple imaging techniques in the same patient poses a great demand for multimodal image registration to show functional and anatomical information on a single interactive fused display. Integration of complementary information provides the foundation for a variety of clinical applications,[1,2] including localization and boundary definition of organs and lesions, comparison of anatomical information with function, planning of radiation therapy, and image-guided surgery.

Computed tomography (CT) and myocardial perfusion single photon emission computed tomography (MPS) convey different characteristics. This is due to the fact that the CT image is created by the attenuation of external photons throughout the thoracic volume, while MPS is created by emissions of photons primarily in the myocardium, with poorly perfused regions exhibiting a reduced photon signal. The advent of multislice CT scanners with rapid rotation has increased the availability of noninvasive coronary CT angiography (CTA), a promising method for cardiac imaging. Contrast-enhanced coronary CTA allows depiction of coronary anatomy and noninvasive assessment of coronary artery stenosis and coronary artery plaque.[3] Recently, it has been suggested that contrast-enhanced cardiac CT can also be

used to detect ischemic heart disease by assessment of rest and stress myocardial perfusion during CTA, but this method of perfusion assessment is not yet in common use.[4] Additionally, MPS is a mainstream imaging technique used to estimate myocardial hypoperfusion due to coronary stenosis,[5] which, however, cannot be observed by MPS directly. Consequently, it is essential to combine different imaging modalities that provide clinically complementary information in the diagnosis, which can be achieved by registration.

It has been proposed that the combination of CTA and MPS modalities can provide clinically complementary information and offer better understanding of perfusion defects,[6–9] and most applications to date utilize manual or semiautomated image fusion for this purpose.[6] For example, visual analysis of fused MPS and coronary CTA images can improve the diagnostic value of sequential combined imaging,[7] and manual tools for coronary CTA-MPS fusion have been developed.[6] However, manual alignment is tedious and observer dependent, which complicates clinical protocols and reduces the practicality of such tools. Nakajo *et al.*[8] proposed a semiautomated coregistration of coronary CTA with gated MPS using a left ventricle (LV) binary model of coronary CTA. In their work, gated single photon emission computed tomography (SPECT) data were registered and mapped to a left ventricle binary model extracted from CTA data using manual, rigid, and affine registration methods with a cost functional of the SPECT count value. However, manual procedures were involved and the potential phase mismatch problem was not addressed although gated SPECT datasets were used for registration. On the other hand, our group was the first to propose a preliminary automated multimodal combination of MPS with coronary CTA scans using presegmented MPS volumes.[9] A preliminary approach from our group[9] has dealt with the phase mismatch problem by assuming that reconstructed CT cardiac phases were obtained from the ED phase and MPS data could be integrated to the ED phase using a "motion-frozen" technique.[10] However, one limitation of this approach was the rigid body assumption, which may be significantly inaccurate when reconstructed cardiac phases differ in the two modalities.

In general, there have been other related studies on the registration of MPS with other cardiac modalities. Faber *et al.*[11] proposed a point-based registration of the MPS surface with 3D coronary anatomy reconstructed from invasive 2D coronary angiography, and it did not use volume registration. Guetter *et al.*[12] developed a registration method for MPS and noncontrast CT data to improve attenuation correction. However, in their study, images were obtained by the hybrid SPECT-CT scanner (in contrast with different stand-alone scanners) where images are already in approximate alignment, requiring only small correction. Guetter *et al.*[12] proposed a learning-based method that exploits the mutual information and an intensity co-occurrence prior. However, this approach used an off-line training process. Besides, all data sets have to be provided *a priori*; otherwise, the prior model may not be incrementally extended as new image data (e.g., different vendors or abnormal data) are available. In related development, Aladl *et al.*[13] proposed an MRI-MPS volume registration technique which utilized the MRI motion to presegment the heart for registration with MPS. However, this approach is not practical for CTA since typically only a few cardiac phases with acceptable image quality may be available for analysis due to radiation dose considerations.

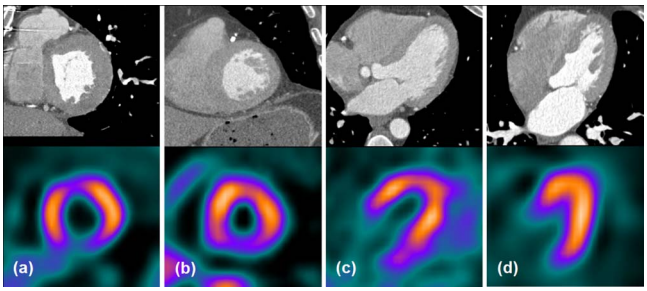

FIG. 1. Examples of CT (top) and MPS (bottom) volume cross sections illustrating image variations between patients: (a) and (b) show coronal views for two different patients. (c) and (d) show the axial/transverse views for the respective patients.

Registration methods can be categorized into two types. "Feature-based" methods rely on local image features such as edges or relevant anatomical structures, whereas "intensity-based" methods directly use image intensity and do not require any additional function for characterizing structures in image. A number of different measures have been applied for the computation of dissimilarity and mutual information and its variant are the most popular approaches, especially for multimodal image registration.[14,15] However, in most cases, intensity alone is often insufficient, and additional information needs to be incorporated. This is especially true for images from abnormal subjects who have inherent physiological variations between different modalities. Consequently, the relationship between two different image characteristics may vary from case to case, and thus derivation of additional prior information may not be effective in this application, since both MPS and cardiac CT datasets have large variations caused by the different injection contrast and perfusion defects, resulting in highly variant intensity distribution, even in the same region. Also, the standard dissimilarity measure for multimodal image registration such as mutual information based method[16] may not be very effective without specialized preprocessing.

In this paper, we aim to develop a fast and fully automated multimodal image registration method for aligning functional MPS with anatomical CT scans by extending our preliminary approach.[9] Accurate registration of contrast-enhanced cardiac CT with MPS is challenging as different anatomical features are visible in different images. For example, although the myocardium is visible on both cardiac CT and MPS, there could be severe perfusion defects present on MPS images which do not have equivalent appearance on CT as shown in Fig. 1. Additionally, variation in the intravenous contrast distribution for different patients causes intensity variations on CT images within the blood pool region.

To alleviate the problems and provide robust registration results regardless of image variations, we proposed to utilize

the explicit and geometrically characteristic information (i.e., segmented boundary of MPS) to find the correspondence and estimate intensity values in the myocardium and blood pool regions simultaneously using a variational framework, where a piecewise constant image model of each segmented region is incorporated as a similarity measure. Both segmentation and registration are interrelated[17] and heavily subject to image characteristics that provide discriminative power between the regions of interest and the background. However, a joint segmentation and registration scheme may not be applicable to our problem since the characteristic features that define the boundary of regions of interest in MPS are usually subtle (especially in abnormal datasets) and this will severely degrade the performance of both segmentation and registration. Consequently, we have proposed an algorithm that applies segmentation as an initial step and subsequently registration procedure.

We first perform rigid registration of the segmented boundary of gated MPS with cardiac CT. Subsequently, the best matching cardiac phase is automatically found based on the cost functional, followed by nonlinear landmark-based warping of gated MPS to the specific phase matching to the CT phase. The nonlinear registration is applied within gated MPS for better visualization of defects to improve spatial resolution and to remove blurring due to motion artifact. To our knowledge, our technique is the first to address the issues of multimodal image registration and cardiac phase matching problem at the same time. In our application, we only use segmentation of MPS images, since cardiac CT has relatively homogeneous intensity distribution compared with MPS volume. Although the degree of contrast between the blood pool and myocardium of cardiac CT varies according to the dataset obtained, the proposed scheme can estimate corresponding intensity values in an alternative manner.

II. MATERIALS AND METHODS

II.A. Description of the method

II.A.1. Preprocessing

A fully automated segmentation algorithm[18] for the LV of gated SPECT previously developed in our laboratory is adopted to define specific regions of interest, including myocardium, blood pool, and extracardiac region, in the MPS volume. In this step, all gated MPS volumes are segmented. This technique has been previously validated[19,20] and provides high accuracy of MPS segmentation.[21] In brief, for each interval of a gated MPS volume, an asymmetric Gaussian is fitted to each profile from which a maximal count midmyocardial surface is determined. The inflection points of the Gaussian are taken to be the surface points.

Geometric features of the boundary of a left ventricle obtained from the segmentation of MPS volumes are of great importance as they can provide the anatomical information to guide registration. Those regions to be extracted from MPS volumes usually do not present distinguished boundary features, resulting in an inhomogeneous intensity distribution within the same anatomical region as shown in Fig. 2.

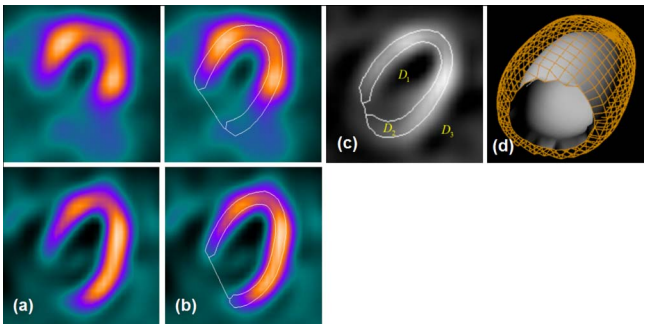

FIG. 2. An example of myocardial segmentation of MPS: (a) shows transverse views for an abnormal case (top) and a normal case (bottom); (b) shows respective contours from segmentation overlaid on the images from (a); (c) illustrates the blood pool (D_1), myocardial (D_2), and extracardiac (D_3) regions; (d) shows 3D contours obtained from the myocardial segmentation, endocardium (surface), and epicardium (mesh). Note the robust segmentation result despite abnormality in MPS.

Let I and J be segmented MPS and cardiac CT volumes, respectively, in Ω, which correspond to an open and bounded domain in $\mathbb{R}^3$. As stated before, we use only segmented MPS volumes due to possible large hypoperfusion abnormalities which would disrupt the cost function. For cardiac CT, we use original intensities with Gaussian smoothing to suppress possible noise and artifacts. Both volumes have a different image size but the transformation is calculated on the same space. The segmented MPS volume I is the union of three disjoint regions; namely, the blood pool, myocardium, and extracardiac structures. We denote regions of blood pool, myocardium, and extracardiac structures by D_1, D_2, and D_3, respectively, where $\Omega = D_1 \cup D_2 \cup D_3$ as shown in Fig. 2(c). We assume that CTA has relatively homogeneous intensity values in blood pool and myocardium and apply a Gaussian-shaped filter of 3 mm standard deviation to the CTA volume to reduce the intensity variation due to noise and lower the CTA image resolution closer to the MPS image.

II.A.2. Registration model

Given preprocessed MPS and CT volumes, we automatically align the centers of the end-diastolic (ED) phase of segmented MPS and the reconstructed CT volume as an initialization step, and then apply the proposed multimodal registration method. An overview of the registration method is presented in Fig. 3.

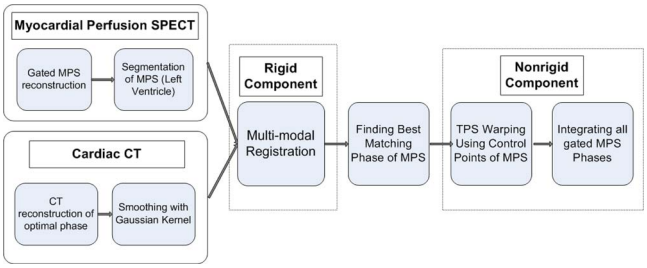

FIG. 3. Overview of the registration procedure.

Our goal in multimodal registration is to estimate the transformation $T_\Theta(\cdot)$ that maps the MPS gated phase to the cardiac CT volume. Transformation $T_\Theta(\cdot)$ is a rigid transfor mation of parameters $\Theta=(t_x,t_y,t_z,\theta_x,\theta_y,\theta_z)$ that denote translations with respect to the x, y, and z directions and rotations around in the x, y, and z axes, respectively. The optimal transformation $\hat{T}_\Theta(\cdot)$ was found by iteratively shifting and rotating the MPS until the energy functional defined in Eq. (1) computed with the two volumes is minimized.

The energy functional based on the segmented MPS volume and CT volume can be defined as

$$\begin{aligned} E(c_1,c_2,c_3,\Theta) &= \int_{D_1} |c_1 - G_\sigma * (J \circ T_\Theta)(x)|^2 dx + \int_{D_2} |c_2 - G_\sigma * (J \circ T_\Theta)(x)|^2 dx + \int_{D_3} |c_3 - G_\sigma * (J \circ T_\Theta)(x)|^2 dx \\ &= \int_\Omega \chi_{D_1}(x) \cdot |c_1 - G_\sigma * (J \circ T_\Theta)(x)|^2 dx + \int_\Omega \chi_{D_2}(x) \cdot |c_2 - G_\sigma * (J \circ T_\Theta)(x)|^2 dx \\ &\quad + \int_\Omega \chi_{D_3}(x) \cdot |c_3 - G_\sigma * (J \circ T_\Theta)(x)|^2 dx, \end{aligned} \tag{1}$$

where * denotes convolution operator, c_1, c_2, and c_3 are constants that approximate the average intensities of regions D_1, D_2, and D_3, respectively, and G_σ is a Gaussian kernel with standard deviation σ, T_Θ is a rigid transformation of six parameters Θ, and $J \circ T_\theta$ is the transformed CT volume. The characteristic function χ_D is defined by

$$\chi_D(x) = \begin{cases} 1, & x \in D \\ 0, & x \notin D. \end{cases} \tag{2}$$

For both CT and MPS volumes, transverse image orientation is used for the registration process.

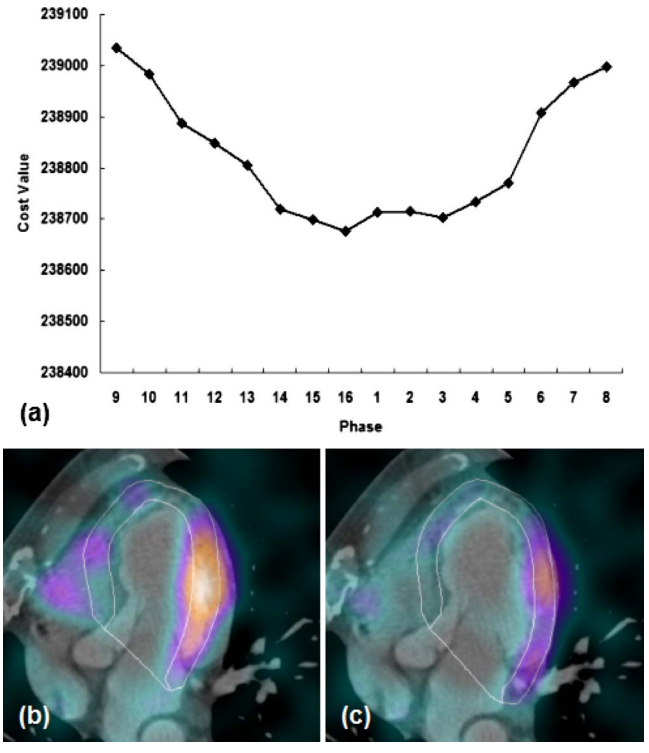

FIG. 4. An example of finding the best matching phase of gated MPS by minimizing the registration cost functional: (a) plot of cost functional value across different phases of MPS; (b) overlaid registration result of phase 9 MPS on CT perfusion; (c) overlaid registration result of best matching phase (16) with CT perfusion. Note that the best matching MPS phase is visually well correlated with CT.

II.A.3. Minimization

The optimal values for the parameters (c_1,c_2,c_3,Θ) that minimize the given energy functional are obtained by solving the associated Euler–Lagrange equations, and a gradient descent method is performed. Parametrizing the descent direction by an artificial time $t \geqslant 0$, the derivation of the Euler–Lagrange equations is given below,

$$\frac{\partial \Theta_i}{\partial t} = -\frac{\partial E}{\partial \Theta_i} (i = 1,2,\ldots,6). \tag{3}$$

In this derivation, we consider only one term in the energy functional for simplicity, which is given by

$$-\frac{1}{2}\frac{\partial E}{\partial \Theta_i} = \int_\Omega \{\chi_D(x) \cdot (c - G_\sigma * (J \circ T_\Theta)(x))\} \cdot \left(\frac{\partial}{\partial \Theta_i} (c - G_\sigma * (J \circ T_\Theta)(x)) \right) dx. \tag{4}$$

By setting $T_\Theta(x) = T(\Theta,x)$, we get

$$\frac{\partial}{\partial\Theta_i}(G_\sigma * (J\circ T_\Theta)(x)) = \int_{\mathbb{R}^2} G_\sigma(y)\frac{\partial}{\partial\Theta_i}\{J(T(\Theta,x-y))\}dy$$

$$= \int_{\mathbb{R}^2} G_\sigma(y)\,\nabla J(T(\Theta,x-y)) \cdot \frac{\partial T(\Theta,x-y)}{\partial\Theta_i}dy. \quad (5)$$

Furthermore, by setting $\partial J\circ T_\Theta(x)/\partial\Theta = L_t(\Theta,x) = \nabla J(T(\Theta,x))\cdot\partial J(\Theta,x)/\partial\Theta$, we obtain

$$\frac{\partial}{\partial\Theta_i}(G_\sigma * (J\circ T_\Theta)(x)) = \int_{\mathbb{R}^2} G_\sigma(y)L_i(\Theta,x-y)dy \quad (6)$$

$$= G_\sigma * L_i(\Theta,x).$$

Hence, Eq. (3) becomes

$$-\frac{1}{2}\frac{\partial E}{\partial\Theta_i} = \int_\Omega \{\chi_D(x)\cdot(c - G_\sigma * (J\circ T_\Theta) \cdot (x))\}G_\sigma * L_i(\Theta,x)dx. \quad (7)$$

By keeping Θ fixed, the minimization of the energy E with respect to constants c_1, c_1, and c_3 leads to

$$\begin{cases} c_1 = \dfrac{\int_\Omega \chi_{D_1}(x)\cdot(G_\sigma * (J\circ T_\Theta)(x))dx}{\int_\Omega \chi_{D_1}dx} \\ c_2 = \dfrac{\int_\Omega \chi_{D_2}(x)\cdot(G_\sigma * (J\circ T_\Theta)(x))dx}{\int_\Omega \chi_{D_2}dx} \\ c_3 = \dfrac{\int_\Omega \chi_{D_3}(x)\cdot(G_\sigma * (J\circ T_\Theta)(x))dx}{\int_\Omega \chi_{D_3}dx}. \end{cases} \quad (8)$$

The constant intensity values and transformation parameters can be minimized using Eqs. (7) and (8) in an alternative manner. We employ a coarse-to-fine multiresolution scheme for computational efficiency and robustness.

II.A.4. Cardiac phase matching with thin-plate-spline warping

It is necessary to match cardiac phases between MPS and CT since the reconstructed CT cardiac phase may vary. Consequently there could be a mismatch between cardiac phases of two modalities, which might affect further visual analysis and image registration. To match the cardiac phase between these two modalities, we perform rigid registration of gated MPS to CT, using the ED phase of MPS (since cardiac CT is usually reconstructed in diastole), and then evaluate the cost functional value for all the other phases of gated MPS. Subsequently, the best matching phase of MPS can be selected according to the cost value where the minimum value is found,

$$k^* = \arg\min_{k\in\{1,\ldots,n\}} E_k(c_1,c_2,c_3,\Theta), \quad (9)$$

where k denotes phase number, n is total number of phase, and $E_k(c_1,c_2,c_3,\Theta)$ denotes the cost functional defined in Eq. (1) with phase k of MPS. In Fig. 4, we illustrate one example of cardiac phase matching, where phase 16 is the best matching phase of MPS (defined as the smallest cost value). By using cardiac phase matching, it can be clearly seen that both the modalities are aligned more accurately as shown in Fig. 4(c).

In what follows, derived LV contours are used in combination with nonlinear registration to compensate for phase mismatch, thereby creating the average MPS volume, warped to the best matched cardiac phase that best corresponds to CT. For the nonlinear registration, 3D thin-plate-spline[22] (TPS) is used to model the nonlinear deformation between all image phases of gated MPS and the best matching cardiac phase position. This is similar to the motion-frozen technique[10] which is also previously developed by our group. This nonlinear registration step is applied only within gated MPS data for better visualization of defects.

More specifically, once detection of epi- and endocardial surfaces on the gated MPS images is accomplished using the technique previously developed,[18] the contour points are positioned on vectors normal to the myocardial surface. These corresponding points are used as template and target control points to be registered where the control points are kept unchanged. Let P denote a template shape surface and Q a target shape surface. We assume that P_L, the landmarks in the template shape P, are known and fixed. Given n control points in a template volume $\hat{p}=(p_x,p_y,p_z)\in\Re^3$, the TPS finds a mapping f from P_L to corresponding landmarks Q_L, $\hat{q}=(q_x,q_y,q_z)\in\Re^3$, on the target surface Q. The thin-plate bending energy, which measures the required energy to deform a volume to match these two sets of landmarks, is then characterized by

$$d(P_L,Q_L) = \int\int\int_{-\infty}^{\infty} L(f)dxdydz, \quad (10)$$

where

$$L(\cdot) = \left(\frac{\partial^2}{\partial x^2}\right)^2 + \left(\frac{\partial^2}{\partial y^2}\right)^2 + \left(\frac{\partial^3}{\partial z^2}\right)^2 + 2\left(\frac{\partial^2}{\partial x\partial y}\right)^2 + 2\left(\frac{\partial^2}{\partial y\partial z}\right)^2 + 2\left(\frac{\partial^2}{\partial z\partial x}\right)^2.$$

The thin-plate bending energy is invariant under any affine transformation. The TPS model is a transformation that is able to represent elastic deformation. Successive TPS-based transformations f_1 through f_{N-1} are computed for phases, that map I_1 through I_{N-1}, respectively, to I_N which is the best matching phase corresponding to the CT phase as shown in

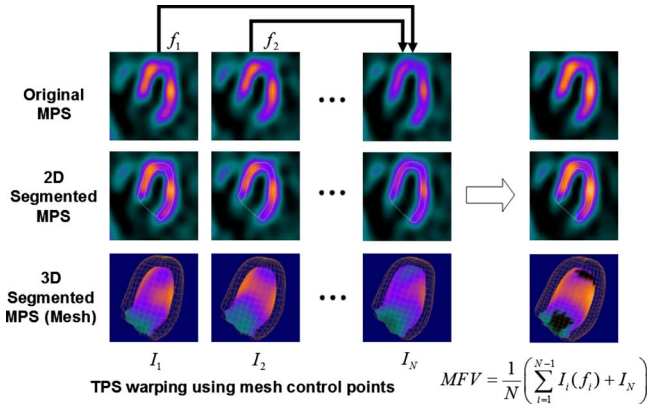

FIG. 5. "Motion-frozen" technique: All MPS frames are registered to a common reference frame I_N, which is the best matching MPS phase for the CT volume. TPS-based warping (T_i) is used to deform and map each frame to I_N. The control points from the segmentation contours serve as landmark points for TPS warping and corresponding points from the source and target contours determine the mapping. Final motion-frozen image is obtained by averaging over all the warped volumes. Note that perfusion defects are clearly seen in the final image (final column).

Fig. 5. The final motion-frozen volume (MFV) can be given as

$$MFV = \frac{1}{N}\left(\sum_{i=1}^{N-1} I_i(f_i) + I_N\right). \quad (11)$$

Note that perfusion defects are observed more clearly in Fig. 5 (final column) using the cardiac phase matching and the TPS warping that is applied individually to each phase, for all the cardiac phases. All the registered image frames are then integrated to represent a final motion-frozen volume in the cardiac phase, which corresponds to the CT phase. For example, for a 16-phase gated dataset, 15 image phases are registered to the best matching phase.

II.B. Validation

II.B.1. Patient selection

Between 1 October 2005 and 31 May 2007, we retrospectively identified 35 consecutive patients (26 men and 9 women; mean age 67 ± 12 years) who underwent myocardial MPS and coronary CTA within a 90 day period at Cedars-Sinai Medical Center (site A) or a neighboring outpatient imaging center (Cardiovascular Medical Group of Southern California, Beverly Hills, California) (site B). All had full datasets available for processing. Additionally, we also retrospectively identified five patients who underwent MPS and stress CT angiography for assessment of myocardial perfusion within 30 days at site A. This study was approved by the Institutional Review Board at Cedars-Sinai Medical Center.

II.B.2. Coronary CTA: Acquisition and reconstruction

Coronary CTA was performed on the SOMATOM Definition dual-source CT (DSCT) scanner (Siemens Medical Systems, Forchheim, Germany) at site A and by a Lightspeed VCT 64-slice CT scanner (GE Healthcare, Waukesha, WI) at site B. Prescan beta-blockade was performed at both sites to attain a heart rate <70 beats/min (<60 beats/min at site B). At site A, ECG-gated helical CTA was performed during a 10–12 s breath hold by injecting 92 ml of intravenous contrast and using scan parameters of heart-rate dependent pitch (range of 0.2–0.45), 330 ms gantry rotation time, 83 ms temporal resolution, 0.6 mm slice thickness, 120 kVp tube voltage, and 600 mA s tube current. At site B, ECG-gated helical CTA was performed during a 9–12 s breath hold by injecting 100 ml of intravenous contrast and using scan parameters of heart-rate dependent pitch, 350 ms gantry rotation time, 0.625 mm slice thickness, 120 kVp tube voltage, and 300–700 mA tube current depending on patient size. At both sites, ECG-based dose modulation was used for all patients to limit radiation dose. The specifications of reconstruction at both sites are given as follows.

Site A. Retrospectively gated reconstruction of raw CTA data was routinely performed at 40%, 65%, 70%, 75%, and 80% of the R-R interval using the following parameters: 0.6 mm slice thickness (0.75 mm if BMI >35 kg/m^2), 0.3 mm slice increment, 250 mm field of view, 512×512 matrix, and B26f medium smooth kernel. Reconstructed data for the cardiac phase with the best quality were transferred to a separate Windows workstation via DICOM protocol for coronary CTA-SPECT fusion.

Site B. Raw data from 5% phases of the cardiac cycle representing 40%–80% of the R-R interval were reconstructed with 0.625 mm slice thickness, and 250 mm field of view, using single-segment reconstruction and a standard convolution kernel. The matrix size was 512×512 with a transverse pixel spacing of 0.49 mm/pixel. Reconstructed data for the 75% phase were transferred to a separate Windows workstation via DICOM protocol for coronary CTA-SPECT fusion.

II.B.3. Stress CT perfusion: Acquisition and reconstruction

Patients enrolled in the CT perfusion study were part of an IRB-approved pilot study at the Cedars-Sinai Medical Center (site A). Under this protocol, patients with perfusion defects in their MPS study were recruited for a stress CT perfusion study within 1 month of their MPS scan. Adenosine (Adenosine, Astellas Pharma, Illinois, US, Inc.) was infused over 5 min at a constant rate of 0.14 mg min^{-1} kg^{-1}. At the end of 3 min of adenosine infusion, contrast-enhanced CT was performed as described in Sec. II B 2. From this contrast-enhanced stress CT scan, the best-quality cardiac phase was identified (either 70% or 40% for the patients in this study, depending on the heart rate at the time of the scan). Stress CT perfusion series was retrospectively reconstructed from this best-quality cardiac phase with the following parameters: 512×512 matrix, 250 mm field of view, 1 mm slice thickness, 0.5 mm slice increment, and a smooth reconstruction kernel (B10f). The reconstructed stress CT perfusion data were transferred to a separate Windows workstation via DICOM protocol for CTA-SPECT fusion.

II.B.4. Myocardial perfusion SPECT protocol

Rest stress MPS studies were acquired with dual isotope (Tl–Tc) protocol[23] or a low dose-high dose same day Tc protocol.[24] MPS acquisitions were performed with noncircular orbits, obtaining 64 projections over 180° (45° RAO to 45° LPO). Acquisitions were performed on Philips CardioMD or Forte cameras or on Siemens e.cam camera. The stress was performed with exercise, adenosine injection, or adenowalk protocol.[25] No attenuation or scatter correction was used. Gated and summed data were reconstructed with filtered back projection (FBP) and with Butterworth filter (cutoff of 0.83 cycles/cm, order of 5) to original transverse orientation without any short axis reorientation. Site A had 16-bin gated acquisition and site B had 8-bin gated acquisition. The matrix and reconstructed voxel size of MPS are $64\times64\times24$ and $6.4\times6.4\times6.4$ mm, respectively.

II.B.5. Evaluation of automatic registration

To evaluate the performance of the proposed method in terms of the registration accuracy and robustness, we have performed a series of experiments on datasets of 20 stress/rest MPS images and coronary CTA datasets acquired at two different sites (as mentioned above), and additionally 5 stress MPS images and CT perfusion datasets.

The proposed method was also compared to the conventional intensity-based normalized mutual information (NMI) method without any specialized preprocessing. Registration results using the proposed registration method and NMI based method were compared with manual alignment by two expert observers.

Each image $S:D\mapsto[0,1]$ is associated with a probabilistic model by introducing a local random variable X, which is uniformly distributed in D, and its related intensity random variable $S(X)$. For registration, CT images were chosen as the reference images $M:D_M\mapsto[0,1]$, and MPS images were chosen as the floating images $N:D_N\mapsto[0,1]$. The transformation is represented by a mapping $T_\Theta:D_N\mapsto D_M$ which belongs to Hilbert space. The joint intensity distribution of $M(X)$ and $N(T_\Theta(X))$ in the overlap region $V=D_N\cap T_\Theta^{-1}(D_M)$ can be estimated from pixel samples using Parzen window given by

$$p(m,n;T)=\frac{1}{|V|}\int_V \phi\left(\frac{m-M(x)}{\rho}\right)\phi\left(\frac{n-N(x)}{\rho}\right)dx, \qquad (12)$$

where ϕ is a Gaussian kernel and ρ determines the width of the window.

The joint histogram and NMI can be defined to represent the global statistics between two images and have been widely employed for multimodal image registration and proven to be less sensitive than mutual information to changes in the region of overlap.[26] The joint histogram H and NMI N are defined as follows:

$$H(M,N;T)=-\int\int p(m,n;T)\log p(m,n;T)dmdn, \qquad (13)$$

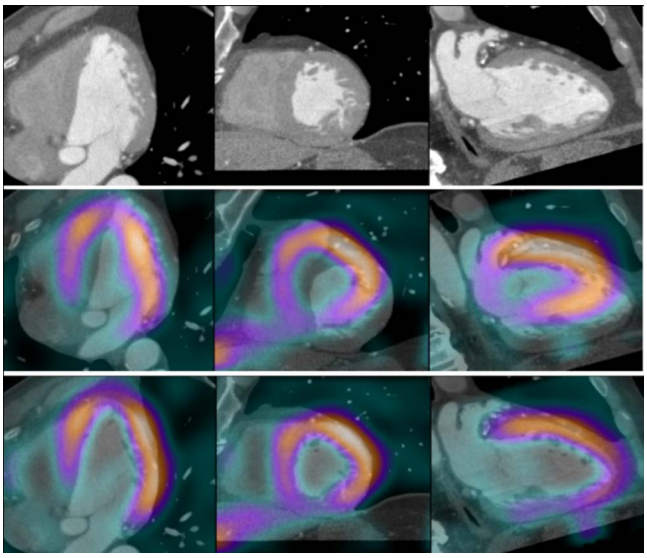

FIG. 6. An example of registration results: original CT image (top), images before (middle), and after (bottom) registration are shown. Errors were 2, 1, and 0 mm for translation and 1°, 1°, and 0° for rotation, as compared to visual alignment.

$$N(M,N;T)=\frac{H(M;T)+H(N;T)}{H(M,N;T)}. \qquad (14)$$

In our experiment, we set the number of histogram to 10, kernel bandwidth ρ to 0.4, and number of sample size to 10% of the total pixel number. Additionally, two levels of multiresolution optimization were performed for both the NMI based method and the proposed method. The algorithm stops when translation is less than 0.01 mm or iteration reaches the predefined iteration number of 50 in both methods.

The registration errors were measured by absolute difference of six parameters $\Theta=(t_x,t_y,t_z,\theta_x,\theta_y,\theta_z)$ between manual alignment and results obtained from the two methods. We tested the datasets under the same initialization conditions. For all the datasets, multiple registrations were done with different initializations (translations of −100–100 mm in each direction with step size of 10 mm) away from the ground truth to measure the capture range.

III. RESULTS

The registrations were performed on an Intel Core2 Duo CPU with a clock speed of 2.5 GHz and 4 GB memory. The mean computation time for the whole process of the proposed method was 7.6 ± 0.4 s (1.1 s for segmentation, 3.2 s for rigid registration, and 3.3 s for TPS warping to the best matching phase). The NMI based method had a larger error than the proposed method and the average registration time was higher 14.8 ± 8.6 s. Our registration of MPS with cardiac CT achieved a success rate of 87% (6 failed out of 45 datasets). Registration failure is defined by the error bigger than 10 mm. Examples of the coronary CTA and MPS pair and registration results of CT perfusion-MPS registration are shown in Figs. 6 and 7, respectively.

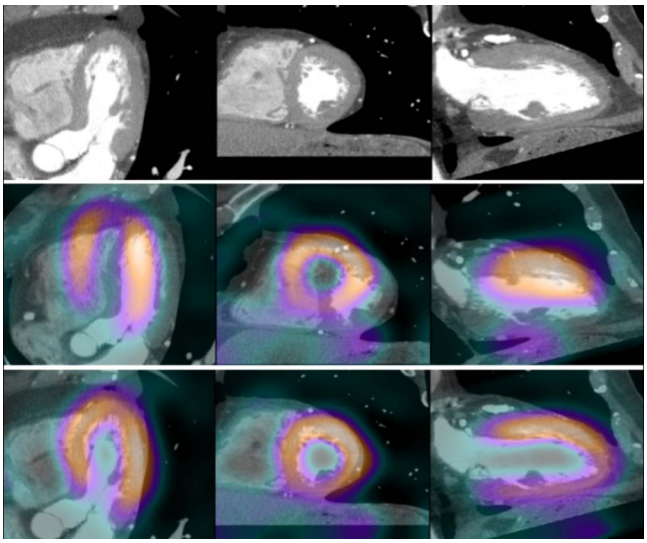

FIG. 7. An example of registration results (CT perfusion): original CT image (top), images before (middle), and after (bottom) registration are shown. Errors were 1, 0, and 4 mm for translation and 5°, 2°, and 3° for the rotation, as compared to visual alignment.

Figure 8 plots the translational probes for registering one representative example case of CT perfusion using the proposed method and NMI based method. Figure 8(a) plots the result using NMI based method and its NMI values with different offsets from the ground truth as visually determined are presented in Fig. 8(b) and Fig. 8(c) plots the result using the proposed method with different offsets and its cost values are presented in Fig. 8(d).

The translational and rotational registration results were not much different in interobserver variability and in the stress and rest MPS (p=NS) as shown in Table I. No significant differences were observed between the two different coronary CTA/MPS protocols, as shown in Fig. 9. That is, 4.3 ± 3.7, 3.6 ± 3.6, and 3.6 ± 2.1 mm for translation and $2.1 \pm 3.2°$, $0.3 \pm 0.9°$, and $0.7 \pm 1.2°$ for rotation for site A and 3.8 ± 2.6, 4.0 ± 3.4, and 2.2 ± 2.3 mm for translation and $1.1 \pm 2.0°$, $1.6 \pm 3.1°$, and $1.9 \pm 3.8°$ for rotation for site B (p=NS). The results of CT perfusion were 3.0 ± 2.9, 3.5 ± 2.4, and 2.8 ± 1.0 mm for translation and $3.0 \pm 2.4°$, $0.6 \pm 0.9°$, and $1.2 \pm 1.3°$ for rotation. In Fig. 9 and Table I, we have compared the different registration results with different data sets. The result shows that the proposed method performed better than the NMI based method in translation, and similarly in terms of rotation. In these results, we excluded the six failed cases. In Table II, we present validation results of finding the best cardiac matching phase by the algorithm as compared with the visual ground truth obtained from an expert observer. It can be observed that best matching phases were not different by more than two phases, as visually determined.

In Figs. 10 and 11, we have presented the plots of capture range of each axis with different misalignments, which shows the proposed method is robust with different initializations compared to NMI based method. Average of five cases was computed according to the offset misalignment introduced along each axis. The proposed method provided robust results using different initializations of translation in the ranges from −80 to 70, −80 to 70, and −50 to 50 mm from the manual ground truth in the x-, y-, and z-axes, respectively. As shown in Fig. 11, the capture range of the NMI based method was much smaller than the proposed method in the ranges from −20 to 20, −20 to 20, and −10 to 40 mm in the x-, y-, and z-axes, respectively.

IV. DISCUSSION

In this study, we proposed and evaluated a fully automated method to register cardiac CT (anatomical information) to MPS (physiological information). Anatomical features, segmentations of LV in the MPS volume, were automatically found in advance to guide the registration process. With a piecewise constant image model, both volumes were then registered using the region-based sum of squared difference as the similarity measure. The best matching phase of MPS was subsequently selected based on the minimum cost value, followed by the TPS warping using derived LV contours to match all image phases of gated MPS to the best matching cardiac phase position (i.e., the best corresponding to the CT phase). As compared with existing methods, we provided a correct solution to the compensation of the moving heart using the TPS-based warping within gated MPS. This is the first report describing both the registration and the phase mismatch problems. The proposed methods were validated on MPS and cardiac CT (coronary CTA and CT perfusion) obtained from multiple MPS cameras and two CT scanners.

TABLE I. Registration error and interobserver variability.

		Translation (mm)			Rotation (°)		
		X	Y	Z	X	Y	Z
NMI based	Stress	9.5 ± 8.2	8.8 ± 6.7	8.5 ± 6.2	1.8 ± 2.7	1.1 ± 2.3	1.6 ± 3.0
Method	Rest	7.3 ± 5.6	10.6 ± 8.6	12.7 ± 6.5	2.0 ± 3.8	1.1 ± 2.5	3.1 ± 1.5
Proposed	Stress	4.6 ± 3.4	4.0 ± 3.0	2.9 ± 2.1	1.7 ± 2.6	0.9 ± 2.3	1.4 ± 3.1
Method	Rest	4.3 ± 3.2	3.8 ± 2.4	3.8 ± 2.4	1.8 ± 3.3	0.1 ± 0.3	0.3 ± 0.7
Interobserver	Stress	3.7 ± 2.4	3.5 ± 2.8	2.2 ± 1.8	3.5 ± 3.1	1.9 ± 3.0	3.1 ± 2.8
Variability	Rest	4.3 ± 2.6	3.8 ± 3.1	3.2 ± 2.9	3.0 ± 3.5	1.8 ± 3.1	2.9 ± 4.7

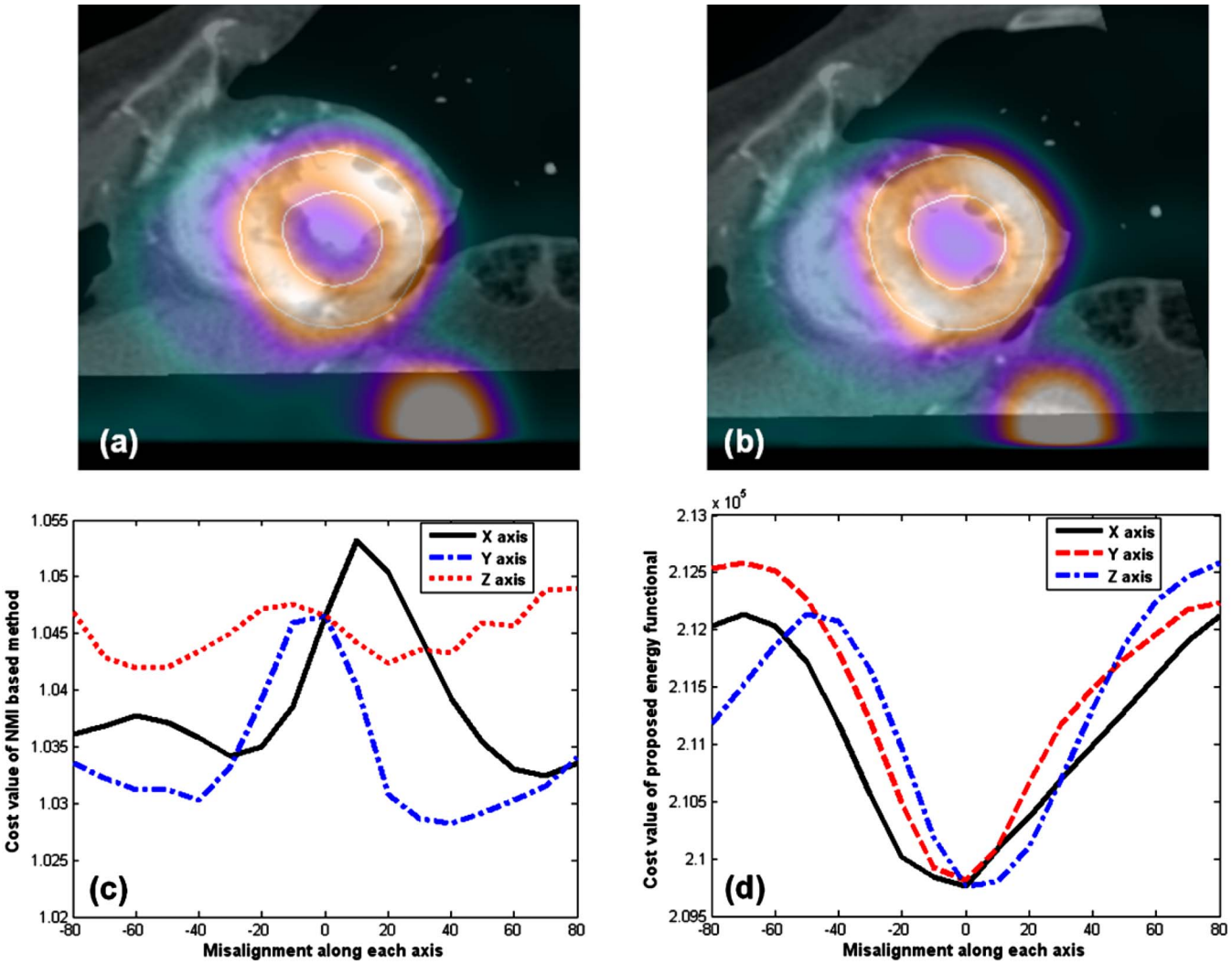

FIG. 8. Comparison of NMI based method and proposed method: (a) registration result using NMI based method; (b) registration result using the proposed method; (c) the NMI values for translational offsets from the ground truth for each axis; (d) the cost values of proposed method for translational offsets from the ground truth for each axis. Note that the anatomical features are very different and the image segmentation will aid the registration of MPS to CT. Additionally, cost value of the proposed method is optimal at the origin, whereas NMI does not provide any such robust optimum.

The evaluation of our algorithm was performed with the rigid registration scheme. The subsequent nonlinear registration was applied only within gated MPS data for the visualization purposes to improve spatial resolution and to remove blurring due to motion artifact. Consequently, the registration performance should be measured by the registration scheme with rigid registration while the nonlinear registration scheme is solely aimed for better visualization in the observation of defects. Robust and accurate registration accuracy was obtained with respect to the ground truth, as visually determined by two expert observers. The translational error was less than the size of a MPS voxel, and therefore is feasible to be used for the clinical practice. For rotations in rigid registration, a small time step in the minimization step was adopted to constrain the angular movement to $-2°$ to $2°$, since both cardiac CT and MPS were acquired in a similar posture. Furthermore, the best matching phase was also validated using visual assessment from an expert observer. Registration of the patient data achieved 87% success rate with accuracy <10 mm. As for the robustness test, the capture range was used. The capture range represents the range of positions from which a registration method can converge to the correct minima/maxima. The proposed method provided a more robust capture range as compared with that of the NMI based method. We additionally have presented validation of best matching phase method compared to visual assessment obtained from an expert observer. Best matching phases found by our proposed method were not different by more than two phases, as visually determined. These results are acceptable since visual assessment is not absolute and in some cases it was equivocal to find only one phase that corresponds to CT phase, as visually determined.

In general, as compared with brain image registration, both cardiac image registration and its validation are inherently more difficult because of cardiac and respiratory motion.[27] Consequently, rigid registration alone may not be sufficient, and subsequent nonlinear component should be used to compensate for changes in organs or tissue due to the

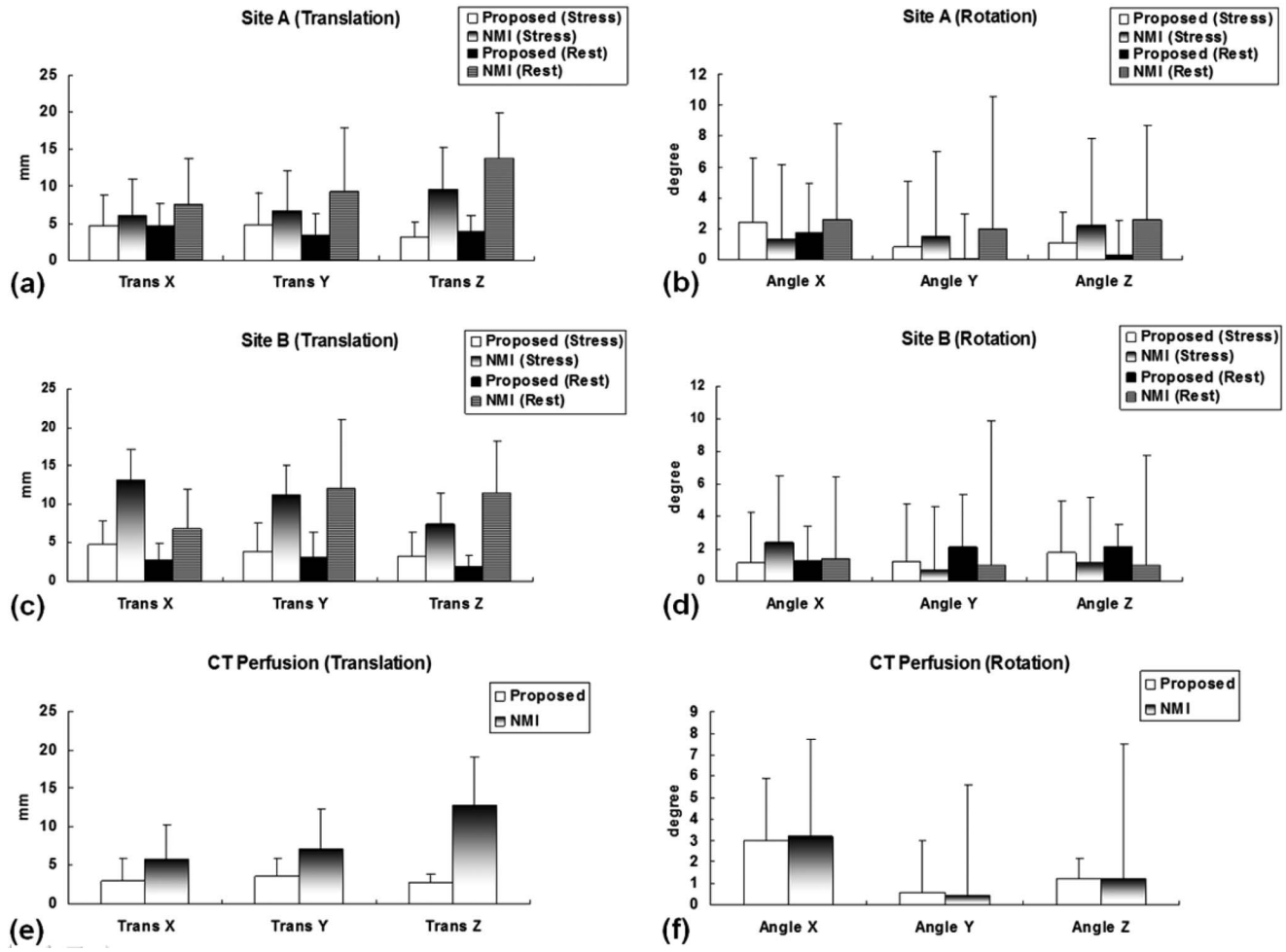

FIG. 9. Registration errors: (a) translational errors of stress/rest MPS and CT obtained from site A; (b) rotational errors of stress/rest MPS, and CTA obtained from site A; (c) translational errors of stress/rest MPS, and CT obtained from site B; (d) rotational errors of stress/rest MPS, and CT obtained from site B; (e) translational errors of stress/rest MPS and perfusion CT; (f) rotational errors of stress/rest MPS and perfusion CT.

breathing pattern or movement of internal organs. Since the exact ground truth is unknown and only visual judgment is available, quantitative evaluation of the registration is challenging and subject to interobserver variability. No significant differences were observed between interobserver variability and the results of the proposed method.

Our proposed method might have potential limitations. First, we applied surface-based registration using segmentation of left ventricle in MPS. However, this contour-driven approach will admittedly affect the registration accuracy when it comes to the poor segmentation result of MPS. In our system, if the MPS contours are not correct, they are manually adjusted for the perfusion and fusion analyses of MPS; therefore from the practical standpoint correct segmentation will be available in all cases, even if adjusted manually for purposes of MPS analysis. However, in our experiment, no manual segmentation adjustment aided by user was observed. Secondly, there are several possible image artifacts such as windmill artifact that might affect the performance of the proposed method. However, the patients in this study were without known coronary artery disease, and patients with existing coronary artery bypass grafts were excluded from the study. There were no datasets that had any metallic implants. For CTA data, we performed Gaussian smoothing to suppress noise and artifacts. We have previously published systematically categorized image artifacts in our patient population, and percentage of patients with artifacts due to metallic implants was 3%,[28] suggesting that our proposed method will not be subject to this difficulty in the vast majority of applicable patients. In our experiment, there were six failed cases. The reason for failure was that all six datasets have large atria with different blood pool sizes between CT and MPS rather than the artifacts present. These datasets can be considered as outliers of our assumption that each region should be corresponding in terms of size and constant intensity level.

Although SPECT/CT scanners become more widely available, there are two reasons why it will be preferable to perform register MPS and CTA images acquired on standalone machines rather than perform a hybrid MPS/CTA scan. Firstly, current SPECT/CT scanners are configured with lower performance CT scanners. Typically it is a CT machine capable of attenuation correction or calcium scoring but not of high-speed resolution CT angiography. SPECT/CT is not

TABLE II. Evaluation of best matching phase.

Patient No.	Stress/Rest	Visual ground truth (phase/total phase)	Our method (phase/total phase)
1	Stress	5/8	7/8
	Rest	6/8	7/8
2	Stress	5/8	7/8
	Rest	6/8	7/8
3	Stress	5/8	7/8
	Rest	7/8	8/8
4	Stress	6/8	7/8
	Rest	6/8	7/8
5	Stress	8/8	8/8
	Rest	1/8	1/8
6	Stress	7/8	7/8
	Rest	1/8	7/8
7	Stress	5/8	6/8
	Rest	5/8	7/8
8	Stress	8/8	7/8
	Rest	8/8	7/8
9	Stress	14/16	15/16
	Rest	16/16	16/16
10	Stress	1/16	15/16
	Rest	15/16	16/16
11	Stress	14/16	14/16
	Rest	12/16	11/16
12	Stress	2/16	1/16
	Rest	2/16	1/16
13	Stress	2/16	1/16
	Rest	2/16	1/16
14	Stress	14/16	16/16
	Rest	15/16	16/16
15	Stress	1/16	1/16
	Rest	2/16	1/16
16	Stress	16/16	16/16
	Rest	16/16	1/16
17	Stress	16/16	1/16
	Rest	14/16	16/16
18	Rest	6/16	6/16
19	Stress	1/16	15/16
20	Stress	1/16	15/16
21	Stress	1/16	16/16
22	Stress	8/16	8/16

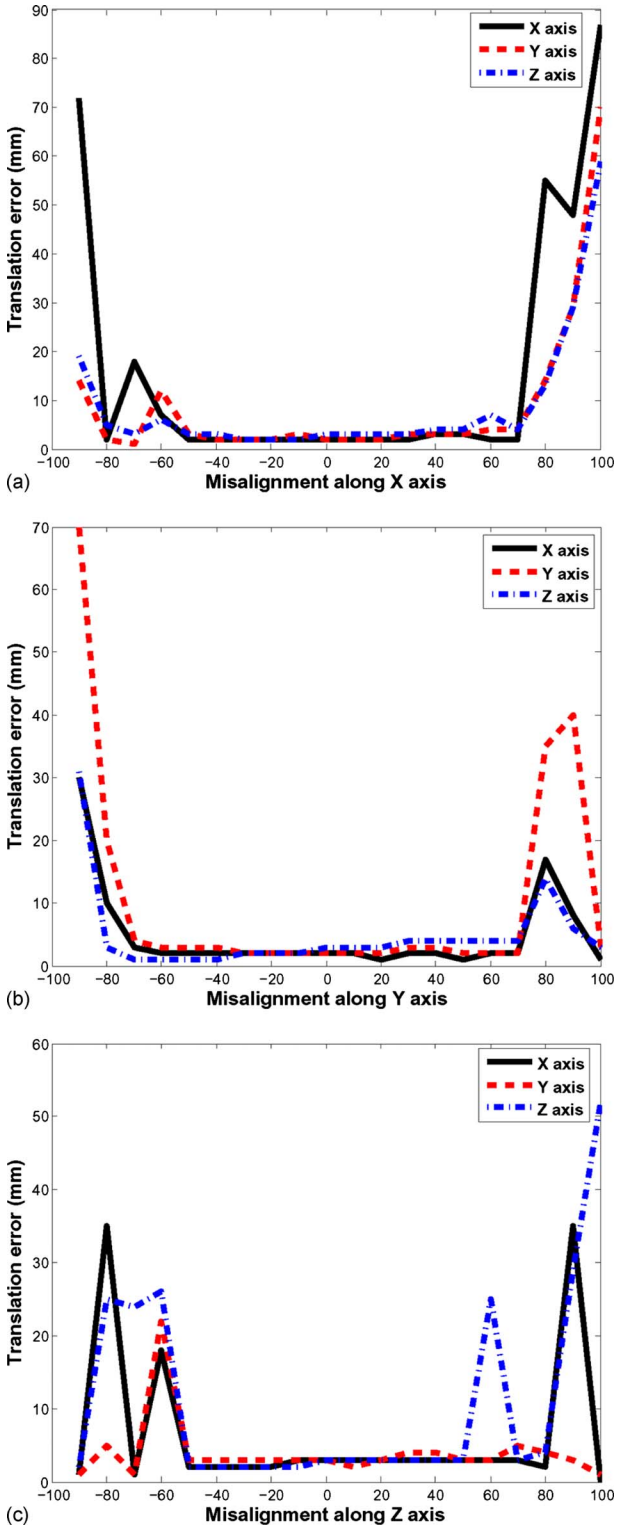

FIG. 10. Capture ranges of the proposed method: (a) translation errors for different misalignment initializations along x axis; (b) translation errors for different misalignment initializations along y axis; (c) translation errors for different misalignment initializations along z axis.

offered in with 64-slice scanners which are preferred for CT angiography. Secondly, from the clinical point of view it is most valuable to know the results of one test before deciding if additional test (and additional radiation dose) is required. For example, when the results are equivocal for CTA in case of heavily calcified arteries, a second test such as MPS can be ordered to resolve the diagnostic question—but this cannot be predicted before the test. On a hybrid SPECT/CT machine it would be difficult to modify the protocol on the fly based on the intermediate results of one test and therefore the use of standalone modalities is more practical clinically. The selective application of one of these tests or a combination as presented here will be most cost effective as it will allow minimizing the ionizing radiation dose. In addition, even if MPS and CTA were performed in the same scanning session on the hybrid scan, there will likely be residual registration errors during the respiratory differences, since CT angiography is performed during a breath hold while MPS is

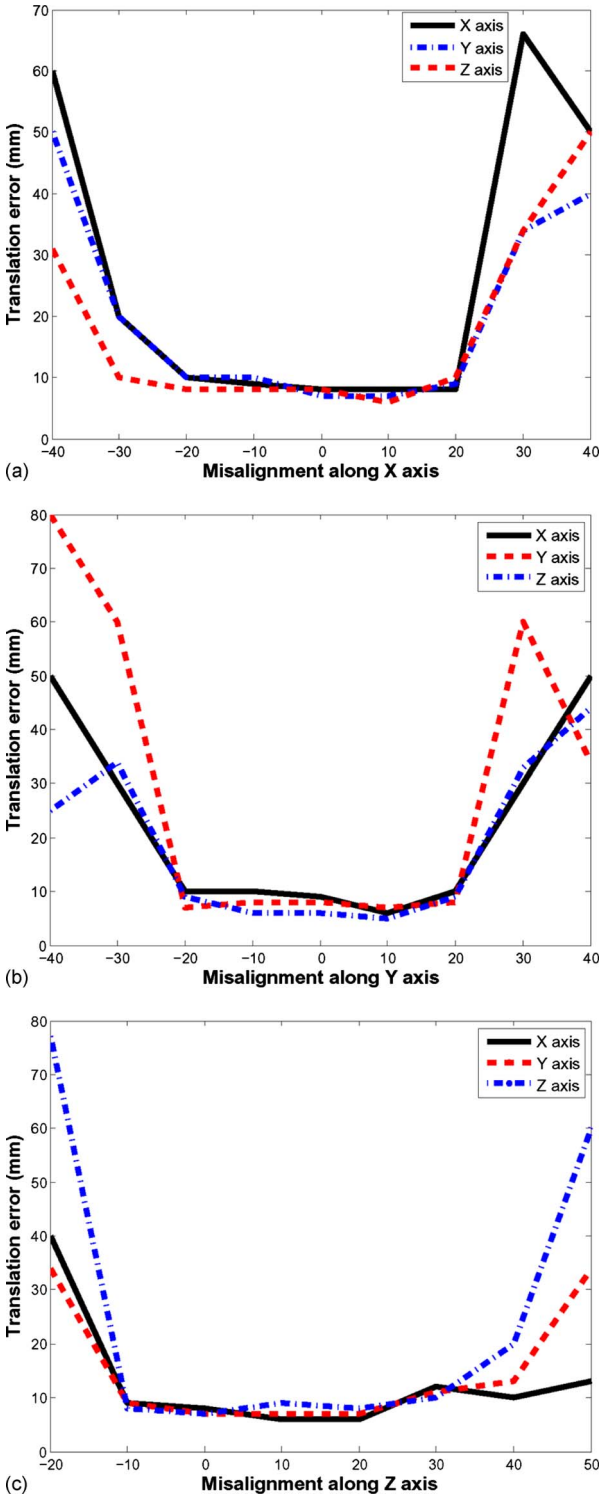

FIG. 11. Capture ranges of the NMI based method: (a) translation errors for different misalignment initializations along x axis; (b) translation errors for different misalignment initializations along y axis; (c) translation errors for different misalignment initializations along z axis.

performed during normal breathing and software image registration as presented here may still be required.

The proposed technique can also be extended to PET-CT fusion since the segmentation technique has been applied and use in for PET imaging.[29] Consequently, after PET segmentation, the registration problem would be essentially the same as for MPS, since no raw MPS data are used in the registration.

V. CONCLUSIONS

A multimodal image registration method of cardiac CT with SPECT in a variational framework was presented. A segmentation method for extracting the blood pool, myocardium, and extracardiac structures from MPS was adopted prior to registration. In the registration process, these segmented regions in MPS were aligned to the corresponding regions in contrast CT by utilizing geometrically characteristic features obtained by MPS segmentation and the homogeneity property of intensities within regions of interest in contrast CT. A specialized cost functional for matching segmented heart image to cardiac CT was designed.

We demonstrated by experimental results that the proposed method outperformed a standard registration method based on normalized mutual information. The results show that the proposed approach provides fast, accurate, and robust registration with error less than the size of a MPS voxel as tested in datasets from two different sites obtained with three different acquisition protocols. This fully automated method may facilitate integrated gated SPECT and cardiac CT analysis to resolve borderline cases in clinical practice, while reducing operator time and variability needed for manual adjustments.

ACKNOWLEDGMENT

Byung-Woo Hong was partly supported by the National Research of Korea (NRF) grant funded by the Korea government (MEST) (No. 2009-0082064).

[a]Electronic mail: piotr.slomka@cshs.org

[1]P. J. Slomka, D. S. Berman, and G. Germano, "Applications and software techniques for integrated cardiac multimodality imaging," Expert Rev. Cardiovasc. Ther. **6**, 27–41 (2008).
[2]P. J. Slomka and R. P. Baum, "Multimodality image registration with software: state-of-the-art," Eur. J. Nucl. Med. Mol. Imaging **36**, S44–S55 (2009).
[3]S. Achenbach, "Cardiac CT: state of the art for the detection of coronary arterial stenosis," Journal of Cardiovascular Computed Tomography **1**, 3–20 (2007).
[4]R. Blankstein, D. R. Okada, J. A. Rocha-Filho, F. J. Rybicki, T. J. Brady, and R. C. Cury, "Cardiac myocardial perfusion imaging using dual source computed tomography," Int. J. Cardiovasc. Imaging **25**, 209–216 (2009).
[5]D. S. Berman, L. J. Shaw, R. Hachamovitch, J. D. Friedman, D. M. Polk, S. W. Hayes, L. E. J. Thomson, G. Germano, N. D. Wong, K. Xingping, and A. Rozanski, "Comparative use of radionuclide stress testing, coronary artery calcium scanning, and noninvasive coronary angiography for diagnostic and prognostic cardiac assessment," Semin Nucl. Med. **37**, 2–16 (2007).
[6]O. Gaemperli, T. Schepis, V. Kalff, M. Namdar, I. Valenta, L. Stefani, L. Desbiolles, S. Leschka, L. Husmann, H. Alkadhi, and P. A. Kaufmann, "Validation of a new cardiac image fusion software for three-dimensional integration of myocardial perfusion SPECT and stand-alone 64-slice CT angiography," Eur. J. Nucl. Med. Mol. Imaging **34**, 1097–1106 (2007).
[7]O. Gaemperli, T. Schepis, I. Valenta, L. Husmann, H. Scheffel, V. Duerst, F. R. Eberli, T. F. Luscher, H. Alkadhi, and P. A. Kaufmann, "Cardiac image fusion from stand-alone SPECT and CT: clinical experience," J. Nucl. Med. **48**, 696–703 (2007).
[8]H. Nakajo, S. Kumita, K. Cho, and T. Kumazaki, "Three-dimensional registration of myocardial perfusion SPECT and CT coronary angiogra-

phy," Ann. Nucl. Med. **19**, 207–215 (2005).
[9]J. Woo, P. J. Slomka, D. Dey, V. Cheng, A. Ramesh, B.-W. Hong, D. S. Berman, C.-C. J. Kuo, and G. Germano, "Automated Multi-modality," *IEEE International Symposium on Biomedical Imaging (ISBI)* (Boston, 2009).
[10]P. J. Slomka, H. Nishina, D. S. Berman, X. Kang, C. Akincioglu, J. D. Friedman, S. W. Hayes, U. E. Aladl, and G. Germano, ""Motion-frozen" display and quantification of myocardial perfusion," J. Nucl. Med. **45**, 1128–1134 (2004).
[11]T. L. Faber, C. A. Santana, E. V. Garcia, J. Candell-Riera, R. D. Folks, J. W. Peifer, A. Hopper, S. Aguade, J. Angel, and J. L. Klein, "Three-dimensional fusion of coronary arteries with myocardial perfusion distributions: clinical validation," J. Nucl. Med. **45**, 745–753 (2004).
[12]C. Guetter, M. Wacker, C. Xu, and J. Hornegger, "Registration of cardiac SPECT/CT data through weighted intensity co-occurrence priors," Medical Image Computed Computer Assisted Intervention (MICCAI) **10**, 725–733 (2007).
[13]U. E. Aladl, G. A. Hurwitz, D. Dey, D. Levin, M. Drangova, and P. J. Slomka, "Automated image registration of gated cardiac single-photon emission computed tomography and magnetic resonance imaging," J. Magn. Reson Imaging **19**, 283–290 (2004).
[14]E. D'Agostino, F. Maes, D. Vandermeulen, and P. Suetens, "A viscous fluid model for multimodal non-rigid image registration using mutual information," Med. Image Anal. **7**, 565–575 (2003).
[15]W. M. Wells III, P. Viola, H. Atsumi, S. Nakajima, and R. Kikinis, "Multi-modal volume registration by maximization of mutual information," Am. J. Med. Qual. **1**, 35–51 (1996).
[16]J. P. Pluim, J. B. Maintz, and M. A. Viergever, "Mutual-information-based registration of medical images: a survey," IEEE Trans. Med. Imaging **22**, 986–1004 (2003).
[17]A. Yezzi, L. Zollei, and T. Kapur, "A variational framework for integrating segmentation and registration through active contours," Med. Image Anal. **7**, 171–185 (2003).
[18]G. Germano, H. Kiat, P. B. Kavanagh, M. Moriel, M. Mazzanti, H. T. Su, K. F. Van Train, and D. S. Berman, "Automatic quantification of ejection fraction from gated myocardial perfusion SPECT," J. Nucl. Med. **36**, 2138–2147 (1995).
[19]G. Germano, J. Erel, H. Lewin, P. B. Kavanagh, and D. S. Berman, "Automatic quantitation of regional myocardial wall motion and thickening from gated technetium-99m sestamibi myocardial perfusion single-photon emission computed tomography," J. Am. Coll. Cardiol. **30**, 1360–1367 (1997).
[20]G. Germano, P. B. Kavanagh, and D. S. Berman, "An automatic approach to the analysis, quantitation and review of perfusion and function from myocardial perfusion SPECT images," Int. J. Card. Imaging **13**, 337–346 (1997).
[21]Y. Xu, P. Kavanagh, M. Fish, J. Gerlach, A. Ramesh, M. Lemley, S. Hayes, D. S. Berman, G. Germano, and P. J. Slomka, "Automated quality control for segmentation of myocardial perfusion SPECT," J. Nucl. Med. **50**, 1418–1426 (2009).
[22]F. L. Bookstein, "Principal warps: Thin-plate splines and the decomposition of deformations," IEEE Trans. Pattern Anal. Mach. Intell. **11**, 567–585 (1989).
[23]D. S. Berman, H. Kiat, J. D. Friedman, F. P. Wang, K. van Train, L. Matzer, J. Maddahi, and G. Germano, "Separate acquisition rest thallium-201/stress technetium-99m sestamibi dual-isotope myocardial perfusion single-photon emission computed tomography: a clinical validation study," J. Am. Coll. Cardiol. **22**, 1455–1464. (1993).
[24]C. L. Hansen, R. A. Goldstein, O. O. Akinboboye, D. S. Berman, E. H. Botvinick, K. B. Churchwell, C. D. Cooke, J. R. Corbett, S. J. Cullom, S. T. Dahlberg, R. S. Druz, E. P. Ficaro, J. R. Galt, R. K. Garg, G. Germano, G. V. Heller, M. J. Henzlova, M. C. Hyun, L. L. Johnson, A. Mann, B. D. McCallister, Jr., R. A. Quaife, T. D. Ruddy, S. N. Sundaram, R. Taillefer, R. P. Ward, and J. J. Mahmarian, "Myocardial perfusion and function: single photon emission computed tomography," J. Nucl. Cardiol. **14**, e39–60 (2007).
[25]D. S. Berman, X. Kang, S. W. Hayes, J. D. Friedman, I. Cohen, A. Abidov, L. J. Shaw, A. M. Amanullah, G. Germano, and R. Hachamovitch, "Adenosine myocardial perfusion single-photon emission computed tomography in women compared with men. Impact of diabetes mellitus on incremental prognostic value and effect on patient management," J. Am. Coll. Cardiol. **41**, 1125–1133 (2003).
[26]C. Studholme, D. L. G. Hill, and D. J. Hawkes, "An overlap invariant entropy measure of 3D medical image alignment," Pattern Recogn. **32**, 71–86 (1999).
[27]T. Makela, P. Clarysse, O. Sipila, N. Pauna, Q. C. Pham, T. Katila, and I. E. Magnin, "A review of cardiac image registration methods," IEEE Trans. Med. Imaging **21**, 1011–1021 (2002).
[28]D. Dey, C. J. Lee, M. Ohba, A. Gutstein, P. J. Slomka, V. Cheng, Y. Suzuki, S. Suzuki, A. Wolak, L. Le Meunier, L. E. Thomson, I. Cohen, J. D. Friedman, G. Germano, and D. S. Berman, "Image quality and artifacts in coronary CT angiography with dual-source CT: initial clinical experience," Journal of Cardiovascular Computed Tomography **2**, 105–114 (2008).
[29]W. M. Schaefer, C. S. Lipke, B. Nowak, H. J. Kaiser, P. Reinartz, A. Buecker, G. A. Krombach, U. Buell, and H. P. Kuhl, "Validation of QGS and 4D-MSPECT for quantification of left ventricular volumes and ejection fraction from gated 18F-FDG PET: comparison with cardiac MRI," J. Nucl. Med. **45**, 74–79 (2004).